Spatio-temporal soil moisture retrieval at the catchment-scale using a dense network of cosmic-ray neutron sensors

Maik Heistermann[1], Till Francke[1], Martin Schrön[2], and Sascha E. Oswald[1]

[1]Institute of Environmental Science and Geography, University of Potsdam, Karl-Liebknecht-Straße 24–25, 14476 Potsdam, Germany
[2]UFZ – Helmholtz Centre for Environmental Research GmbH, Dep. Monitoring and Exploration Technologies, Permoserstr. 15, 04318, Leipzig, Germany

Correspondence: Maik Heistermann (maik.heistermann@uni-potsdam.de)

Abstract.

Cosmic-Ray Neutron Sensing (CRNS) is a powerful technique to retrieve representative estimates of soil water content at a horizontal scale of hectometers (the "field scale") and a depth of tens of centimeters ("the root zone"). This study demonstrates the potential of the CRNS technique to obtain spatio-temporal patterns of soil moisture beyond the integrated volume from isolated CRNS footprints. We use data from an observational campaign between May and July 2019 which featured a dense network of more than 20 neutron detectors with partly overlapping footprints in an area that exhibits pronounced soil moisture gradients within one square kilometer. The present study is the first to combine these observations in order to represent the heterogeneity of soil water content at the sub-footprint scale as well as between the CRNS stations. First, we apply a state-of-the-art procedure to correct the observed neutron count rates for static (heterogeneity in space, e.g. soil organic matter) and dynamic effects (heterogeneity in time, e.g. barometric pressure). Based on the homogenised neutron data, we investigate the robustness of a calibration approach that uses one single calibration parameter across all CRNS stations. Finally, we benchmark two different interpolation techniques in order to obtain space-time representations of soil moisture: first, Ordinary Kriging with a fixed range; second, we complement the concept of spatial interpolation by the idea of a geophysical inversion ("constrained interpolation"). To that end, we optimize the parameters of a geostatistical interpolation model so that the error of the forward-simulated neutron count rates is minimized, and suggest a heuristic forward operator to make the optimization problem computationally feasible. The comparison with independent measurements from a cluster of soil moisture sensors (SoilNet) shows that the constrained interpolation approach is superior in representing horizontal soil moisture gradients at the hectometer scale. The study demonstrates how a CRNS network can be used to generate coherent, consistent, and continuous soil moisture patterns that could be used to validate hydrological models or remote sensing products.

1 Introduction

1.1 The retrieval of soil water content from cosmic ray neutrons

The observation of soil water content remains a scientific challenge. Many methods allow for the pointwise measurement of soil water content, but their spatial representativeness is limited when the small spatial measurement support in the order of centimeters (Blöschl and Grayson, 2000) is confronted with a high small-scale variability of soil moisture. Remote sensing, in turn, can provide area-integrated measurements, but is typically limited by shallow penetration depths, low overpass frequencies, and the interference of vegetation and surface roughness, to name only a few.

Over the past decade, Cosmic-Ray Neutron Sensing (CRNS) has been established as a powerful alternative to retrieve volume-integrated estimates of soil water content (Zreda et al., 2008; Desilets et al., 2010; Zreda et al., 2012). These estimates are considered as representative for a footprint that extends horizontally over several hectometers (the "field scale"), and vertically over several decimeters ("the root zone"), at a temporal resolution of 3–12 hours (Schrön et al., 2018), depending on detector sensitivity and altitude, for instance. The method relies on measurements of the ambient density of "epithermal" neutrons (at energies of $1–10^5$ eV) above the ground which is inversely related to the presence of hydrogen and hence soil moisture (Köhli et al., 2020).

The soil water content is mostly inferred from the intensity of epithermal neutrons by using a transfer function such as the one suggested by Desilets et al. (2010), and requires the calibration of a parameter N_0 on independent measurements of soil water content in the footprint of a neutron detector (see Schrön et al., 2017, for a recent synthesis). The value of N_0 is affected by a variety of factors, including topography, spatial heterogeneity of soil water content, and the sensitivity of the detector (Fersch et al., 2020a; Schrön et al., 2018), but also the occurrence of hydrogen in snow (Schattan et al., 2017), vegetation (Baroni and Oswald, 2015), lattice water, litter (Bogena et al., 2013), or soil organic carbon.

1.2 Beyond soil moisture retrieval in isolated sensor footprints

Until today, CRNS studies have mainly focused on "isolated" sensor footprints. As an extension to that approach, CRNS roving has demonstrated potential to detect patterns of soil water content along transects across the landscape (Schrön et al., 2018, see, e.g.,). Yet, roving can just produce snapshots in time, and the choice of transects is typically limited by the network of accessible pathways - which could reduce the representativeness of soil moisture estimates especially due to the influence of the road material (Schrön et al., 2018).

The present study aims to explore another approach to continuously monitor the spatial distribution of the soil water content at a horizontal scale of hectometers. The main idea is to cover an area of interest with a dense network of stationary CRNS sensors, and to translate soil moisture estimates from individual footprints into consistent space-time representations of soil moisture across a study domain. The term "dense" suggests that the footprints of the CRNS sensors should ideally overlap, or at least adjoin each other, which implies that the distances between the sensors should be in the order of one footprint radius.

In order to allow for such an investigation, a field campaign had been carried out from May to July 2019. It featured more than 20 neutron detectors (from different manufacturers, with different detection techniques and sensitivities) in an area of

just $1\,km^2$, the Upper Rott catchment. This area is characterised by strong spatial heterogeneity with regard to land use (forest vs. meadows), soil (mineral vs. organic), terrain (hill slopes vs. valley bottom), and the existence of below-ground structures with low permeability. During the campaign, the soil water content was highly dynamic: the soils were saturated after an exceptionally wet May, followed by a general period of drying in June and July, that was interrupted, from time to time, by short events of heavy rainfall.

Recently, all data collected in this campaign have been made available to the public (Fersch et al., 2020a). The present study is the first to explore this unique data set regarding its potential to retrieve space-time representations of soil water content at the hectometer scale.

1.3 Specific objectives

The specific questions addressed in this study are the following:

1. Given the heterogeneity with regard to detector sensitivity and the spatial distribution of hydrogen pools: *can we find a joint value of the calibration parameter N_0 (Eq. 1) for all CRNS sensors?* That way, we could consistently convert observed neutron intensities to soil moisture across all sensors. This requires to homogenise the observed neutron count rates for factors which are heterogeneous in space (e.g. vegetation biomass) or dynamic in time (e.g. barometric pressure). We will examine how the uncertainty of these factors affects the robustness of our N_0 estimation.

2. *What do the differences between the CRSN-based soil moisture estimates tell us about catchment-scale soil moisture patterns and their temporal dynamics?* To address this question, we explore the soil moisture estimates obtained from the observed neutron count rates by using a joint N_0 value, and hence the spatio-temporal variation of soil moisture across the dense CRNS network.

3. *How does soil moisture vary within and between the sensor footprints?* To address this question, we examine two different interpolation techniques: first, the CRNS-derived soil moisture estimates are interpolated using Ordinary Kriging with a fixed range. Second, we introduce a new approach that extends the concept of spatial interpolation by the idea of a geophysical inversion (see e.g. Zhdanov, 2015). To that effect, we optimize the parameters of a geostatistical model by minimizing the disagreement between observed and the forward-simulated neutron count rates. We compare the resulting soil moisture maps to independent Frequency Domain Reflectometry (FDR) measurements from a SoilNet cluster.

1.4 Manuscript structure

The manuscript is structured as follows: in section 2, we briefly introduce the study site, and, in section 3, the data used in the present study (for a comprehensive description see Fersch et al., 2020a). In section 4, we outline the various processing steps required to address the above research questions (homogenisation of neutron counts, calibration of N_0 and the estimation of CRNS-based soil moisture series, and the spatial interpolation of these estimates). We then present and discuss the corresponding results in section 5, and draw conclusions in section 6.

2 Study site

The Fendt study site, at an altitude of around 595 m ASL, is located in the headwater of the Rott river (Fig. 1). The catchment has an area of about 1 km^2, and is part of the TERENO Pre-Alpine Observatory (Kiese et al., 2018; Fersch et al., 2018). A main rivulet drains the catchment from south to north. The hydraulic heads of the shallow aquifers range from 4 to 0.2 m below the ground, with patchy evidence of perched groundwater, though systematic observations are unavailable. The main soil types are Gleysols, Cambisols, Stagnosols, and Histosols (1:25,000 soil survey Bayerisches Landesamt für Umwelt, 2014); the dominant texture classes (Landesamt für Digitalisierung, Breitband und Vermessung, 2018, not surveyed under forest cover) are clay and loam, with substantial patches of peat. Grassland is the most important land use (69 %); a mixed, heterogeneously structured forest (27 %) extends mainly along the eastern slopes of the catchment. An overview of these properties per sensor footprint is provided in Tab. 1.

3 Data

3.1 CRNS measurements

In total, 24 stationary CRNS detectors were positioned in the study area from May to July 2019. For various organisational and technical reasons, some sensors recorded only briefly or patchily. For the present analysis, we only use those 18 sensors which coherently covered at least the majority of the study period including the manual sampling campaign at the end of June 2019. Tab. 1 gives an overview of those sensors, and Fig. 1 shows their locations (see Fersch et al. (2020a) for details about the different detector technologies).

The placement of the CRNS sensors had been based on a set of constraints, some of which scientific, some legal or practical, and some also conflicting with each other (Fersch et al., 2020a): e.g., we aimed to maximise the spatial coverage of the catchment, but also the overlap between sensor footprints. As a compromise, the CRNS sensors were placed more densely in the north-western part of the study area where the SoilNet observations are available for a comparison (see Fig. 1).

The sensitivity of the detectors used in this study ranged over an order of magnitude (between the most sensitive one, NeuSense Dual, and the least sensitive, CRS-1000). However, the effective sensitivity could vary between sensors of the same type, too. In order to standardize neutron count rates across sensors, we had collocated a mobile "calibrator" sensor (#20 in Tab. 1) consecutively beside most of the stationary probes for a duration of at least one day.

As another sensitivity reference, we used mobile CRNS measurements carried out from June 25 to 26. In these two days, a roving CRNS (see Fersch et al., 2020a, for details) was placed next to the stationary CRNS sensors (except sensors 1, 21, and 22 due to inaccessibility) for a duration of at least 30 minutes. The high sensitivity of the roving CRNS allowed count rates to be sufficiently representative to relate them to the count rates of the stationary sensors.
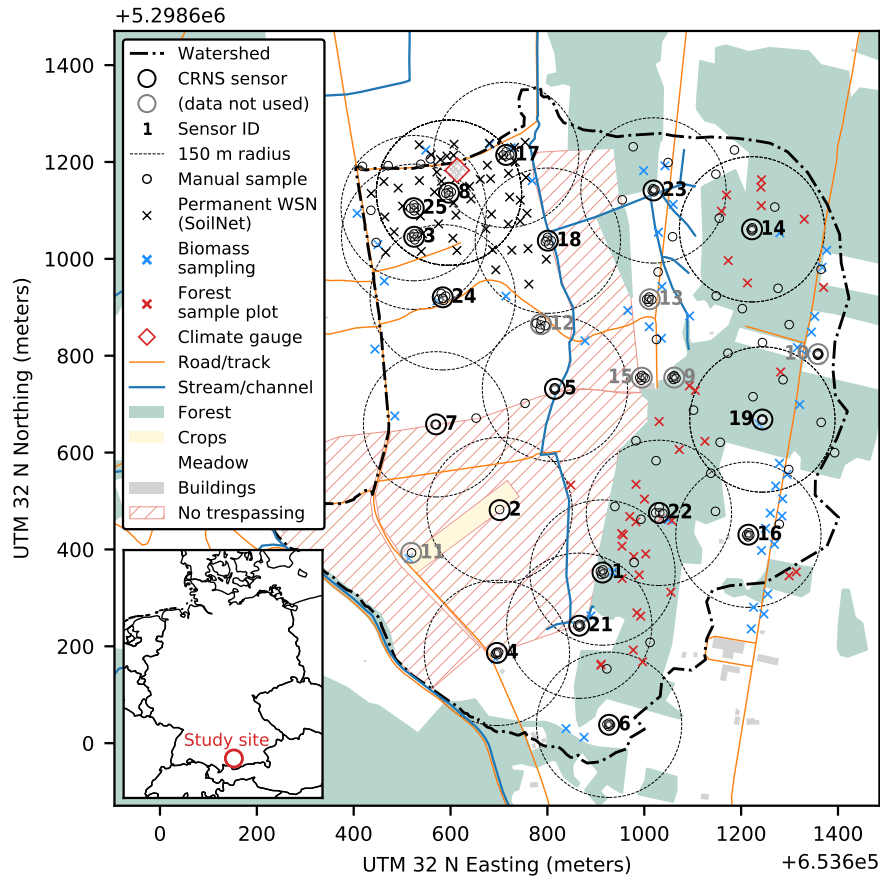
Figure 1. Study area around Fendt with the headwater catchment of Rott river. With regard to land cover, the forest, a few settlements, and a cropland plot are highlighted – the rest is mostly grassland. For instrumentation, we show the CRNS-locations and a typical (Schrön et al., 2017) footprint radius of 150 m, the climate gauge, and the locations of soil moisture measurements from the SoilNet and from the manual measurement campaign from June 25 to 26, 2019. Regarding the latter, typically five manual measurements were carried out in the close vicinity of each CRNS sensor which is difficult to resolve in this map; figure uses OSM basemap layers for waterways, landuse, and roads (© OpenStreetMap contributors, 2020, distributed under ODbL license).

3.2 Incoming cosmic-ray neutron flux and meteorological observations

In order to account for the variation of the incoming cosmic-ray neutron flux, Schrön et al. (2016) recommend to select recordings from neutron monitors which have a similar cutoff rigidity as the study location. In this study, we used the monitor at Jungfraujoch in order to quantify the reference flux. The data was obtained from the Neutron Monitor Database (monitor ID "JUNG", http://www.nmdb.eu).

Table 1. Overview of the 18 CRNS sensors used in this study, including manufacturer, sensor model, detection technology, sensitivity of the sensor relative to the calibrator probe (#20), dominant land use (from OpenStreetMap contributors, 2020), soil texture class (from Landesamt für Digitalisierung, Breitband und Vermessung, 2018, not available under forest) and soil type (from Bayerisches Landesamt für Umwelt, 2014) in the sensor footprint. Please note that the sensor IDs in this table are not consecutively numbered for consistency with Fersch et al. (2020a).

ID	Manufacturer	Sensor model	Technology	Sensitivity	Land use	Soil texture	Soil type
1	Hydroinnova	CRS 2000-B	$^{10}BF_3$	1.190	Forest, meadow	Clay	Gleysols, Cambisols
2	Hydroinnova	CRS 1000	^3He	0.452	Crops, meadow	Clay, some loam	Cambisols, Gleysols
3	Hydroinnova	CRS 1000	^3He	0.458	Meadow	Loam, some clay	Cambisols, Gleysols
4	Lab-C	NeuSens dual	^6Li	4.530	Meadow	Clay and loam	Gleysols, Cambisols
5	Hydroinnova	CRS 1000-B	$^{10}BF_3$	0.670	Meadow	Clay	Gleysols, Cambisols
6	Hydroinnova	CRS 1000-B	$^{10}BF_3$	0.668[*]	Meadow, forest	Clay	Cambisols, Gleysols
7	Hydroinnova	CRS 1000-B	$^{10}BF_3$	0.668[*]	Meadow	Clay, some loam	Cambisols. Gleysols
8	Hydroinnova	CRS 2000-B	$^{10}BF_3$	1.161	Meadow	Loam and clay	Gleysols, Cambisols
14	Hydroinnova	CRS 2000	^3He	0.871	Forest	no data around sensor	Stagnosols, Cambisols
16	Hydroinnova	CRS 2000-B	$^{10}BF_3$	1.148	Meadow	Clay	Stagnosols, Cambisols
17	Hydroinnova	CRS 2000-B	$^{10}BF_3$	1.121	Meadow	Clay, some peat	Gleysols, Histosols
18	Hydroinnova	CRS 1000	^3He	0.414	Meadow	Clay, some peat	Gleysols, Histosols
19	Hydroinnova	CRS 2000-B	$^{10}BF_3$	1.147[*]	Forest	no data around sensor	Gleysols
20	Hydroinnova	Calibrator	^3He	1.000	–	–	–
21	Hydroinnova	CRS 2000-B	$^{10}BF_3$	1.132	Meadow, forest	Clay, some peat	Gleysols, Histosols
22	Hydroinnova	CRS 2000-B	$^{10}BF_3$	1.168	Forest	no data around sensor	Cambisols, Stagnosols
23	Hydroinnova	CRS 2000-B	$^{10}BF_3$	1.127	Meadow, forest	Peat, some clay	Histosols, Cambisols
24	Hydroinnova	CRS 2000-B	$^{10}BF_3$	1.138	Meadow	Clay and loam	Cambisols, Gleysols
25	Hydroinnova	CRS 1000-B	$^{10}BF_3$	0.665	Meadow	Loam, some clay	Cambisols, Gleysols

[*] Calibrator not available, so the sensitivity was obtained from the average values of the same models.

The location of the climate gauge at the Fendt site is shown in Fig. 1. The observed climate variables required for the present analysis include precipitation, barometric pressure, as well as air relative humidity and temperature, recorded at a temporal resolution of one minute.

3.3 Local measurements of soil water content and other soil variables

We require local measurements of soil water content and soil bulk density in order to calibrate the relationship between epithermal neutron intensity and volumetric soil water content. The same holds for the verification of soil moisture retrievals from observed neutron intensities. During the JFC, the following measurement techniques were applied to meet these requirements.

3.3.1 Permanent soil sensor network (SoilNet)

The north-west of the catchment is permanently equipped with a SoilNet (version 3, SoilNet (2018)), a network of 55 vertical sensor profiles (locations shown in Fig. 1). Temperature and permittivity are recorded in depths of 5, 20, and 50 cm, at an interval of 15 minutes, redundantly at each depth with two slightly displaced sensors. Please see Fersch et al. (2020a) for further details on how volumetric soil moisture was obtained from permittivity.

3.3.2 Manual soil sampling and measurement of soil water content

Vertical measurements were carried out from June 25 to 26, 2019, with depth increments of 5 cm down to a maximum depth of 30 cm. Right beside each stationary CRNS sensor, a vertical profile was measured using soil cores and thermo-gravimetry. At another 139 locations at and in-between the stationary CRNS sensors, vertical profiles using the same depths were obtained from manual FDR measurements. Fig. 1 provides an overview of the sampling locations. Please see Fersch et al. (2020a) for a comprehensive description of the sampling scheme, the sample processing for thermo-gravimetry, and the conversion of measured permittivity to volumetric water content for the FDR measurements.

3.4 Vegetation and biomass

For grassland and cropland, above-ground biomass was measured at three dates (May 14–16, June 6 and July 17) at the same 45 locations, and the water content was determined by drying to a constant weight at 65 °C.

For quantifying above-ground biomass in the forest, a different approach was used. Ground-truth information from 116 sites with representative species composition allowed the derivation of a tree-species map using multitemporal RapidEye-imagery. In addition, detailed tree-based surveys at 16 plots (including species, height and breast-height-diameter, see Fersch et al. (2020a) for details) yielded values of above-ground biomass estimates. Using stand-height information from LIDAR, these estimates were generalized for the entire forested area (Stockmann, 2020).

4 Methods

4.1 Homogenisation of neutron intensities in space and time

In order to make the observed neutron count rates comparable across space and time, different effects need to be taken into account, namely the different detector sensitivities, atmospheric effects, and the effects of hydrogen pools other than soil water.

4.1.1 Standardization of sensitivity

Measurements of a collocated calibrator probe (see section 3.1) served to standardize CRNS measurements. For the period of collocation, the ratio between the corresponding stationary and mobile neutron counts was defined as the "sensitivity factor" (constant in time, see Schrön et al., 2018) which was then applied to standardize – to the calibrator level – the neutron intensities

recorded by a stationary detector. In case a calibrator collocation was missing, average values of the same sensor model type were used instead (see Tab. 1).

4.1.2 Accounting for atmospheric effects

The observed neutron count rates are affected by a range of dynamic atmospheric variables that need to be accounted for in order to make neutron intensities comparable across time. These dynamic variables include atmospheric vapor content, barometric pressure, and incoming cosmic-ray neutron flux. To correct for these effects, we used the data mentioned in section 3.2. The corresponding standard correction approach is outlined e.g. by Scheiffele et al. (2020) in Appendix A.

4.1.3 Accounting for the effects of vegetation

We assumed that the spatial variability of above-ground biomass is dominated by the presence of woodland in contrast to grassland: the average above-ground dry matter for grassland and cropland amounted to $0.2\,\mathrm{kg/m^2}$ while the average above-ground dry mass for forested area was quantified as $24.4\,\mathrm{kg/m^2}$ (Stockmann, 2020). The spatial variability of forest biomass turned out to be high. However, its quantification at high spatial resolution (i.e., order of $100\,\mathrm{m^2}$) included considerable uncertainties. Therefore, we decided to use only the *average* above-ground biomass estimates for forest and grassland, respectively. The corresponding spatial distribution of above-ground biomass (in $\mathrm{kg/m^2}$) was represented on a regular grid with a horizontal resolution of $10\,\mathrm{m}$. Based on this grid, we computed the weighted average above-ground dry matter per CRNS sensor footprint by using the horizontal weighting function W_r/r as suggested by Schrön et al. (2017), and assumed these values to be constant throughout the duration of the campaign. On that basis, we accounted for the effect of vegetation on neutron count rates by following Baatz et al. (2015) who suggested "a neutron intensity reduction of $0.9\,\%$ per kg of [dry] biomass per m^2".

4.1.4 Estimating average soil properties per sensor footprint

As pointed out in 3.3.2, the vertical distribution of volumetric water content θ, soil bulk density ρ_b, soil organic matter content SOM, and lattice water content LW was determined at each CRNS sensor from thermo-gravimetry. For volumetric water content, additional vertical profiles were measured using the FDR technique. For the estimation of N_0 (section 4.2), representative averages of these variables had to be obtained for each CRNS footprint. For that purpose, we first approximated the 3-dimensional distribution of soil properties from the available measurements, and then applied the vertical and horizontal weighting functions provided by Schrön et al. (2017) in order to compute weighted averages. In detail, this involved the following steps.

Fit vertical profiles

In order to generalize the vertical distribution of soil variables v_i (i.e. θ, ρ_b, SOM, LW) across the study area, we fitted a piecewise linear function to each profile and variable: from the soil surface ($0\,\mathrm{cm}$) down to a depth of $13\,\mathrm{cm}$, the function assumes a linear change of any variable value from $v_i(0cm)$ to $v_i(13cm)$. Below $13\,\mathrm{cm}$ depth, the variable is assumed to

remain constant at a value $v_i(13cm)$. This approach has been found to reflect the typical vertical distribution pattern for all soil variables fairly well, while reducing spurious effects of outliers when the variables are horizontally interpolated (see next section). Example profiles are illustrated in the Supplement (Figs. S1-S3).

Horizontally interpolate the vertical distribution parameters

The fitted parameters $v_i(0cm)$ and $v_i(13cm)$ at each profile location were then interpolated in space using Ordinary Kriging with an exponential variogram model and a range of 50 m (150 m for soil moisture) on a 10 x 10 m grid (nugget and sill were set to 0 and 1, respectively). Based on the vertical distribution function and the interpolated parameters, we computed the value of the soil variable at 1 cm vertical resolution between 0 and 30 cm. It should be noted that in this study, we applied Ordinary Kriging rather "heuristically" than in a formal geostatistical way: the underlying assumption of stationarity as well as the choice of an exponential variogram model with a specific range was based on the aim to create continuous and plausible spatial patterns that are robust in areas of extrapolation and in which spatial autocorrelation is explicitly considered (instead of implicit assumptions used in techniques such as nearest neighbour, or inverse distance weighting). The sensitivity of our results to the range parameter was explicitly investigated in a Monte-Carlo-analysis (see section 4.3).

For soil organic matter and lattice water, the procedure was modified since both variables had not been determined for each profile separately, but from mixing samples within areas classified as "forest on mineral soil", "other land use on mineral soil" as well as "other land use on organic soil" (see Fersch et al. (2020a)). Hence, the vertical distribution function was only determined for these three classes, and, instead of interpolation, the same vertical profile was assigned to each grid cell based on its membership in one of the three classes.

Compute the weighted average variable value for each sensor footprint

In the final step, we used the weighting functions from Eq. A1 in Schrön et al. (2017) to compute average values of the soil variables per sensor footprint. The vertical average was obtained for each grid cell in the footprint based on the vertical weighting function W_d and the horizontal distance r of the grid cell to the sensor. Then, the vertical averages were averaged horizontally based on the horizontal weighting function W_r/r. As the soil variables of interest are parameters of the weighting functions themselves, the weighting procedure was iterated until the average variables converged (typically after less than 5 iterations), as recommended by Schrön et al. (2017).

4.2 Calibration of N_0

The soil water content is estimated from the epithermal neutron count rate using the standard transfer function suggested by Desilets et al. (2010). This requires the calibration of a parameter N_0 on local soil moisture observations.

$$\theta_g^{all} = \theta_g + \theta_g^{som} + \theta_g^{lw} = \frac{a_0}{N/N_0 - a_1} - a_2 \,, \quad \theta = \frac{\varrho_b}{\varrho_w} \cdot \theta_g \tag{1}$$

In this Eq. 1, subscript g indicates gravimetric soil water (equivalents) in units of kg/kg; hence, θ_g is the gravimetric soil water content, θ_g^{som} and θ_g^{lw} are the gravimetric soil water equivalents of soil organic matter and lattice water, θ is the volumetric soil water content (in m³/m³), ρ_w and ρ_b are the density of water (assumed as 1000 kg/m³) and the soil bulk density (in kg/m³). N is the corrected neutron intensity (in counts per hour, cph), N_0 (in cph) is the calibration parameter. The shape parameters a_0, a_1, and a_2 could be adapted to specific local conditions, but they have also proven to be robust in many previous studies (Desilets et al., 2010; Evans et al., 2016; Schrön et al., 2017, among others), and where set to $a_0 = 0.0808$, $a_1 = 0.372$, and $a_2 = 0.115$. Please note that water equivalents from vegetation (θ_{bio}) are not included in the sum on the left since the effects of vegetation biomass were already accounted for in the corrected neutron intensity N (see section 4.1.3).

In order to use Eq. 1 to compute $\theta_g(N)$ or $\theta(N)$, respectively, from observed neutron count rates N, θ^{som} and θ^{lw} as well as the soil bulk density ϱ_b need to be independently quantified as weighted averages for each CRNS sensor footprint (see section 4.1.4 for details). For any calibration of N_0, θ needs to be independently quantified as calibration reference which we refer to as θ^{obs}. θ_i^{obs} was computed as a weighted average for each CRNS sensor footprint i from manual measurements (section 4.1.4).

Usually, N_0 is calibrated for a single CRNS sensor at a particular site. For our dense cluster, however, we calibrated Eq. (1) by assuming a uniform value of N_0 across the study area. Hence, we optimized N_0 by minimizing the mean absolute difference between the average volumetric soil moisture θ_i^{obs}, and the corresponding $\theta(N_i, N_0)$, that can be obtained by solving Eq. 1 for θ and using the corrected neutron intensities N_i:

$$\operatorname*{arg\,min}_{N_0} \sum_{i=1}^{18} \left| \theta_i^{obs} - \theta(N_i, N_0) \right| \tag{2}$$

The manual soil moisture measurements had been carried out over two consecutive days, June 25-26, 2019 (see section 3.3). Hence, the temporally varying parameters (neutron count rates N_i, barometric pressure, humidity) required as inputs to the weighting functions and Eq. 2 were obtained by computing temporal means between June 25, 08:00 (UTC) and June 26, 18:00 (UTC).

4.3 Exploring the uncertainty of N_0 calibration

Uncertainties in the N_0 estimation arise from errors in the measurement of soil moisture and neutron fluxes as well as the validity and parameterisation of functional relationships and underlying assumptions. In order to get, on the one hand, a better idea about the robustness of our N_0 estimate, and, on the other hand, about the uncertainty of observed and CRNS-based soil moisture, we carried out a Monte-Carlo analysis in which we repeated the N_0 calibration (see Eq. 2) for 200 times, each time with a set of randomly disturbed input parameters (the number of 200 realisations was confirmed to produce sufficiently robust results that also hold for a higher number of realisations). The parameters and disturbances are as follows:

- *Sensor sensitivity*: As pointed out in section 4.1.1, the neutron count rates of all sensors were standardized to the level of a "calibrator". Yet we found some variability of the resulting sensitivity factors even for the same sensor type. In the Monte-Carlo-analysis, we assume the sensitivity to vary by $\pm 2\%$ with respect to the sensitivity level shown in Tab. 1.

- *Averaging period for N_i*: The definition of the time window over which to compute the average neutron intensity N_i is subject to some arbitrariness, particularly since the manual soil moisture measurements took place over a period of two consecutive days (June 25, 08:00 and June 26, 18:00, UTC). In order to capture the effect of the averaging period, we randomly selected 12-hour-windows within this time span, and computed the average N_i from these windows.

- *Dry vegetation matter*: Compared to grassland, the spatial distribution of forest biomass is more relevant in the present study. Stockmann (2020) attempted to represent this distribution by combing allometric approaches and remote sensing, and found the dry matter mass to vary between 13 - 73 kg/m^2, with a relative error of 17 % at the plot scale. As we used one uniform biomass estimate for the forest area (section 4.1.3), we expect large local errors. In our Monte-Carlo-analysis, we vary the dry matter mass per CRNS footprint within $\pm 20\%$ with respect to the estimated value.

- *Water equivalent*: As pointed out in section 4.1.4, soil organic matter and lattice water content were only determined from mixed samples for three different land-use/soil combinations. Hence, the local values for the resulting water equivalents could substantially depart from these average values. Here, we assume the estimated values of θ^{som} and θ^{lw} per footprint to vary within $\pm 20\%$ of the initial estimate.

- *Kriging range*: the choice of using an exponential variogram model together with a specific Kriging range for specific variables was rather arbitrary (section 4.1.4). Hence, we varied the Kriging range values by $\pm 50\%$ of the original values, resulting in a sampling interval between 75 and 225 m for soil moisture, and between 25 and 75 m for bulk density.

- *Subsampling from soil profiles*: For the N_0 calibration, the vertical soil moisture distribution had been sampled at 160 locations in the study area. Given the size of the area and the number of CRNS sensors, the corresponding sample size per CRNS sensor is quite low compared to previous studies (18 samples per footprint were recommended by Zreda et al. (2012)). In order to analyse how the availability of sampling locations affected the N_0 calibration, we employed a sub-sampling approach: for each Monte-Carlo realisation, we used only 80 % of our sampling locations for the interpolation of bulk density and volumetric soil moisture. These 80 % were randomly selected from the entire population of locations.

4.4 Soil moisture retrieval and spatial interpolation

To improve the signal-to-noise ratio for each CRNS sensor, we computed the average neutron count rates at an interval of 24 hours, and then converted, for each CRNS sensor, this averaged neutron count rate to daily volumetric soil water content by using Eq. 1 with the calibrated N_0. This soil water content will be referred to as $\theta(N_i)$ in the following. These values will be examined as a first order representation of how the soil water content varies in the study area in space and time.

In order to represent the spatial soil moisture distribution inside and between CRNS footprints, we interpolate $\theta(N_i)$ to a 10 m x 10 m grid that spans the entire study area. The grid resolution is arbitrarily selected, and does not necessarily reflect the

resolution at which the grid effectively conveys information of spatial heterogeneity; in other words, the product should not be interpreted at the scale of 10 m. Still, we require this comparatively fine horizontal resolution since some of the following steps require to re-aggregate (i.e. to average) the spatial soil moisture estimates inside a CRNS footprint.

Gridded soil moisture estimates are obtained by two spatial interpolation approaches (or "models") which we will refer to as "unconstrained" and "constrained".

4.4.1 Unconstrained model

What we refer to as the "unconstrained" approach could imply any kind of model m that represents the spatial distribution of soil moisture, θ, on the basis of a parameter set $\mathbf{p}$. That could be a geostatistical interpolation approach, or, for instance, a distributed hydrological model.

In this study, we use, as model m, Ordinary Kriging with an exponential variogram model (nugget=0, sill=1) and a range parameter of, say, 300 m, using the CRNS sensor locations as data points for the interpolation. This choice is fairly arbitrary and subjective, but it reflects the spatial scale at which we are interested to represent the variation of soil moisture. With a given number of n CRNS sensors in our study area, our resulting model $m(\mathbf{p})$ will have n parameters, namely the soil moisture θ_i at the CRNS locations i (the data points for the interpolation), the values of which we set to the CRNS-based soil moisture estimates $\theta(N_i)$.

This interpolation approach has one major drawback: it does not account for the consistency between the obtained spatial soil moisture distribution (output of $m(\mathbf{p})$) and the neutron intensities observed at the sensor locations (N_i) (and is hence "unconstrained"). If we were able to simulate the neutron intensities that would correspond to the output of $m(\mathbf{p})$, we would have a basis to *constrain* (or optimize) our parameters $\mathbf{p}$, by maximising the agreement between observed and simulated neutron intensities.

4.4.2 Constrained model

The "constrained" model m is the same as the above "unconstrained", except that we adjust our initial guess of $\mathbf{p}$ such that the disagreement (here the sum of absolute differences) between observed neutron count rates, N_i^{obs}, and simulated count rates, N_i^{sim} (obtained from $m(\mathbf{p})$), is minimized (Eq. 3).

$$\underset{\mathbf{p}}{\arg\min} \sum_{i=1}^{n} \left| N_i^{obs} - N_i^{sim}(m(\mathbf{p})) \right| \tag{3}$$

Fig. 2 A-F illustrates the idea and effects of a constrained model for a simple one-dimensional example with two CRNS sensors and an (unknown) true soil moisture distribution (solid black line, **A**). **B** illustrates the sensor locations together with their horizontal sensitivity pattern (red shadows). Using a suitable forward operator $\mathcal{H}$ (section 4.4.3), we can compute the neutron count rates N_i^{obs} that we would expect the sensors to observe, based on the true soil moisture. These N_i^{obs} constitute the only information we have from our CRNS-sensors. From these N_i^{obs}, we compute the average soil moisture $\theta(N_i^{obs})$, based on Eq. 1 with a known N_0 (**C**). We then apply the unconstrained interpolation by using $\theta(N_i^{obs})$ as data points (θ_i^{node},
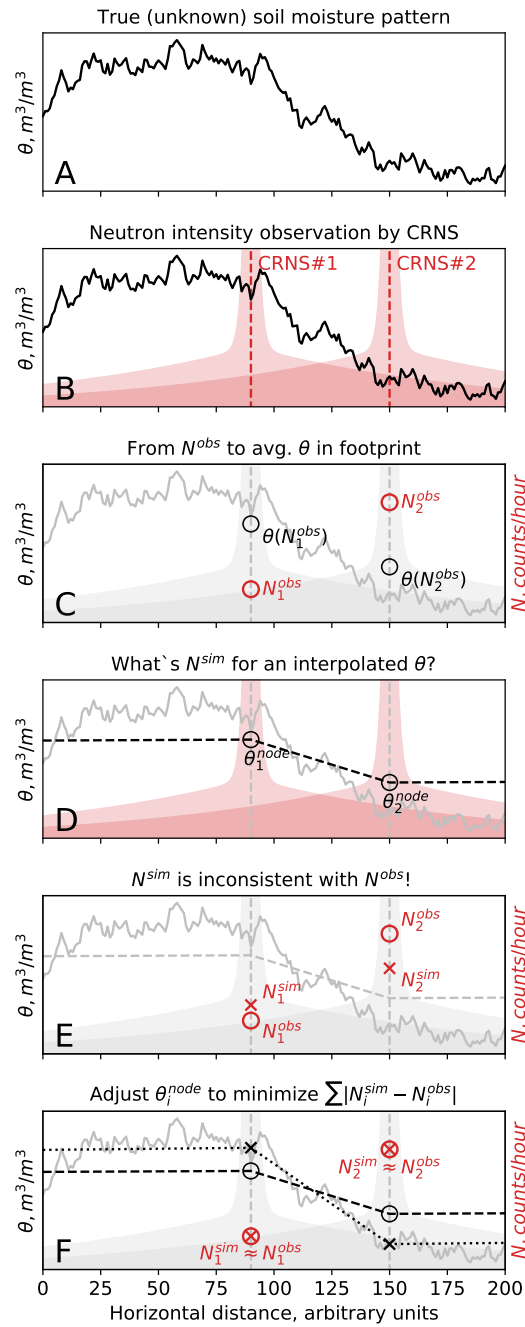
Figure 2. Schematic view of the "constrained" interpolation model, illustrated by an idealized example with two CRNS sensors and a 1-D horizontal soil moisture distribution. Symbols are explained in the main text; note that the spatial domain further extends to the right, but is not entirely shown for the sake of clarity.

D). From the resulting soil moisture distribution (**D**, dashed line), we simulate the corresponding N_i^{sim}, again by using the forward operator $\mathscr{H}$. In the case of a marked soil moisture gradient, as in this example, the resulting N_i^{sim} and observed N_i^{obs} will disagree (**E**). The reason for this disagreement is obvious and unsurprising: using the volume-integrated $\theta(N_i^{obs})$ as a data *point* for the interpolation (θ_i^{node}), we potentially neglect a substantial portion of spatial variation that is hidden behind this volume-average. Hence, spatial gradients will tend to be systematically underrepresented: here, the unconstrained model underestimates areas of high soil moisture in the left half of our spatial domain, and overestimates in the right.

In the "constrained model", we therefore adjust the values for θ_i^{node} so that the disagreement between N_i^{sim} and measured N_i^{obs} is minimized (**F**). This optimisation problem could have an infinite number of equally valid solutions. The problem of equifinality is addressed, however, by using a local optimisation technique (Nelder-Mead Simplex adapted according to Gao and Han, 2012). As our initial parameter guess for (θ_i^{node}) is based on $\theta(N_i^{obs})$, we expect the parameter optimisation to stay close to this initial guess, to change just by as much as required to better represent the local soil moisture gradients. We also expect that the optimisation problem will be constrained better in areas where multiple CRNS sensors have a significant overlap. Conversely, the difference between the initial N_i^{sim} and N_i^{obs} will probably be low for CRNS locations that are rather isolated and distant from others: that is because in the footprint of any isolated (or distant) sensor i, the interpolated soil moisture values will be dominated by $\theta(N_i^{obs})$, and less affected by other sensors.

4.4.3   The forward operator

The constrained model resembles to what is generally referred to as a "geophysical inversion", i.e. the identification of parameters $\mathbf{p}$ in a model m by means of inverse simulation: the observed variable (N) is obtained from the estimated target variable (θ) by means of a physically-based forward operator ("simulation"). Hence, $\mathbf{p}$ is optimised by minimising the disagreement between simulation and observation. That way, further spatial information can be obtained from volume-integrated observations by using our physical understanding of both the observed system and the observation technique itself. On this basis, our "constrained" approach, as outlined above, does not entirely qualify as a "geophysical inversion": first, we use a geostatistical instead of a physical model to describe our notion of soil moisture variation at a specific scale. Second, we use a rather heuristic implementation of a forward operator $\mathscr{H}$ which is specified as follows:

$$\mathscr{H} : \Theta_i^m \mapsto N_i^{sim}, \tag{4}$$

where the operator $\mathscr{H}$ simulates the "corrected" epithermal neutron intensity N_i^{sim} at a sensor location i using the entire environment of interpolated (modelled) soil moisture values, Θ_i^m, in a 300 m radius around the sensor, represented as a grid on which each grid cell j has a modelled soil moisture value θ_j^m.

Shuttleworth et al. (2013) developed the COSMIC operator in the context of data assimilation. However, the COSMIC operator does not account for the horizontal but for the vertical variability of soil moisture, and is therefore not eligible for our purpose. Neutron transport models, in turn, are able to track the histories of millions of neutrons by taking the relevant physical interactions into account, not only including the effects of soil moisture, but e.g. vegetation or topography. Neutron

transport models are available, and have proven valid in a wide range of application contexts. Examples are MCNP (Andreasen et al., 2017), or, more recently, URANOS (Weimar et al., 2020). Both would be suitable forward operators - except that their computational cost is prohibitive in our application context: the optimisation of $\mathbf{p}$ requires hundreds of iterations which would require weeks of computation time – for the soil moisture interpolation at one single point in time alone.

340   Hence, we follow an intermediate approach which we have already referred to as "heuristic": instead of explicitly simulating the physical interactions of neutrons with the near-surface environment, we use the horizontal weighting function W_r that was presented in Eq. A1 of Schrön et al. (2017). W_r represents the horizontal sensitivity pattern of a CRNS sensor, and depends on various environmental, partly dynamic variables such as soil moisture itself, soil bulk density, vegetation, air humidity, and barometric pressure. Though W_r was not originally intended to support forward simulation, it is based on extensive neutron

345 transport simulations (Köhli et al., 2015), and therefore has a sufficient physical basis to serve our main purpose: to quantify, for the observation of neutron intensity at any location i, the relative contribution of soil moisture at different distances from the sensor. W_r, however, does not directly yield neutron intensity (formally, we use it as a spatial filter). Hence, we combine W_r with the inverse of Eq. 1 to obtain a forward operator as represented by Eqs. 5 and 6.

$$N_i^{sim} = \mathscr{H}(\Theta_i^m) = N_0 \cdot \frac{a_0}{\langle \Theta_i^m \rangle \cdot \frac{\rho_w}{\rho_{b,i}} + a_2} + a_1 \qquad (5)$$

350 $$\langle \Theta_i^m \rangle = \frac{\sum_j \left(W_{r,i,j} \cdot \theta_j^m \right)}{\sum_j W_{r,i,j}} + \theta_i^{lw} + \theta_i^{som} \qquad (6)$$

4.5   Comparison to local soil sensor network (SoilNet)

In order to evaluate the performance of the "unconstrained" and the "constrained" interpolation models, the resulting maps of average daily soil moisture are compared against daily soil moisture maps obtained from the FDR-cluster (SoilNet) operated at the site (Fersch et al., 2020a). This comparison, however, is not straightforward: While the SoilNet data consist of a set of

355 observations at specific points in space (with a horizontal support of a few centimeters), results of the interpolation models are spatial soil moisture grids of varying vertical representativeness.

     The SoilNet observations $\theta_{n,z}^{\text{FDR}}$ constitute 55 nodes (index n), each of which provides a measurement at three depths z (5, 20, and 50 cm; the two measurements at each depth are averaged). For each node, we first obtain a continuous vertical profile: we linearly interpolate the measurements at intervals of 1 cm between 5 and 20 cm, and between 20 and 50 cm. Between 5 cm

360 and the soil surface, the value from 5 cm is used. To account for the CRNS penetration depth, we then compute a weighted vertical average $\langle \theta_n^{\text{FDR}} \rangle$ at each node by using the weighting function W_d from Schrön et al. (2017) (note that W_d depends on the distance r to a CRNS sensor which is, however, not unique in case multiple CRNS are present; here, we simply use a "medium" value of $r = 20$ m for all SoilNet nodes since, for average soil moisture values around 0.4 m^3/m^3, the penetration depth only decreases by less than 5 cm within a distance of 100 m from a CRNS, see Fig. 8 in Köhli et al., 2015). Finally,

365 we horizontally interpolate $\langle \theta_n^{\text{FDR}} \rangle$ to the same grid as the interpolated CRNS-based soil moisture, using the same Ordinary Kriging approach as used for the interpolation of CRNS-based soil moisture (exponential variogram with a range of 300 m).

We evaluate the similarity of the spatial soil moisture patterns obtained from the FDR-cluster and the interpolation of $\theta(N_i)$ for each day from May 20 to July 15, 2019. As a measure of similarity, we chose Spearman's rank correlation of the corresponding soil moisture grids. Using that measure, we eliminate potential effects of uncertainty in the soil moisture values obtained from the SoilNet, as the conversion from permittivity to volumetric soil moisture can be subject to systematic bias Mohamed and Paleologos (2018).

5   Results and discussion

5.1   Can we find a uniform N_0 for the entire study area?

Parameter N_0 from Eq. 1 accounts for a variety of factors in the relationship between soil moisture and neutron intensity (e.g. sensor sensitivity, or hydrogen pools other that soil water). N_0 should be the same for each sensor if we had perfectly homogenised the observed neutron intensities with regard to these effects, and if the calibration reference were error-free. Based on our homogenisation efforts (section 4.1 and the successful standardization of sensitivity (as documented in section S2 of the supplementary), we estimated an N_0 value of 3723 cph with a mean absolute error of 0.047 m³/m³ for θ (see Tab. 2 for an overview of calibration input and output). Fig. 3A contrasts CRNS-based soil moisture estimates $\theta(N)$ and the calibration reference θ^{obs}. Fig. 3B illustrates how well the relation between gravimetric soil water content θ_g^{all} and neutron intensity N corresponds to Eq. 1.

While the agreement is not perfect, the general pattern suggests that CRNS-based soil moisture estimates obtained from a single N_0 can explain a substantial portion of variability in the study area ($R^2 = 0.69$) where soil moisture ranges from 0.33 to 0.70 m³/m³. Yet, some sensors display a remarkable disagreement between θ_i^{obs} and $\theta(N_i)$, most notably for sensor 7 (-0.15 m³/m³), but also for sensor 22 (+0.09 m³/m³), sensor 5 (+0.08 m³/m³), and sensor 23 (-0.07 m³/m³).

We would like to put these disagreements into perspective by providing a better idea of the uncertainties involved in the N_0 calibration on June 25-26. Based on the Monte-Carlo analysis (section 4.3), Fig. 4 displays the local uncertainty of $\theta(N_i)$ and θ_i^{obs} (A) as well as N_i and $\theta_{g,i}^{all}$ (B). The term "local" refers to the uncertainty for a specific sensor footprint i (please see figure caption for details).

The results shown in Fig. 4 can be seen as both unfavourable and encouraging. The level of local uncertainties, as expressed by the vertical and horizontal extent of the dark shades, is rather unfavourable. The uncertainty of $\theta(N_i)$ is a location-specific combination of uncertainties, e.g. of the above-ground forest biomass, the mean N_i (which was represented by temporal sub-sampling), or the spatial distribution of soil bulk density. The average uncertainty of $\theta(N_i)$ (i.e. the mean width of the dark boxes along the y-axis) amounts to 0.08 m³/m³. Yet, θ_{obs}, the so-called "ground-truth", bears some uncertainty, too (0.03 m³/m³ on average, for the dark boxes along the x-axis). This uncertainty mainly results from the limited spatial density of the measured profiles.

It is encouraging, though, that the estimation of N_0 appears quite robust, and that there is no evidence to suggest that N_0 is not uniform across sensors (except for sensor 7). The 25th and 75th percentiles of N_0 amount to 3677 and 3733 cph, respectively, which corresponds to a range of less than 1.5 % relative to the optimal value of $N_0 = 3723$ cph (Fig. 4C). The
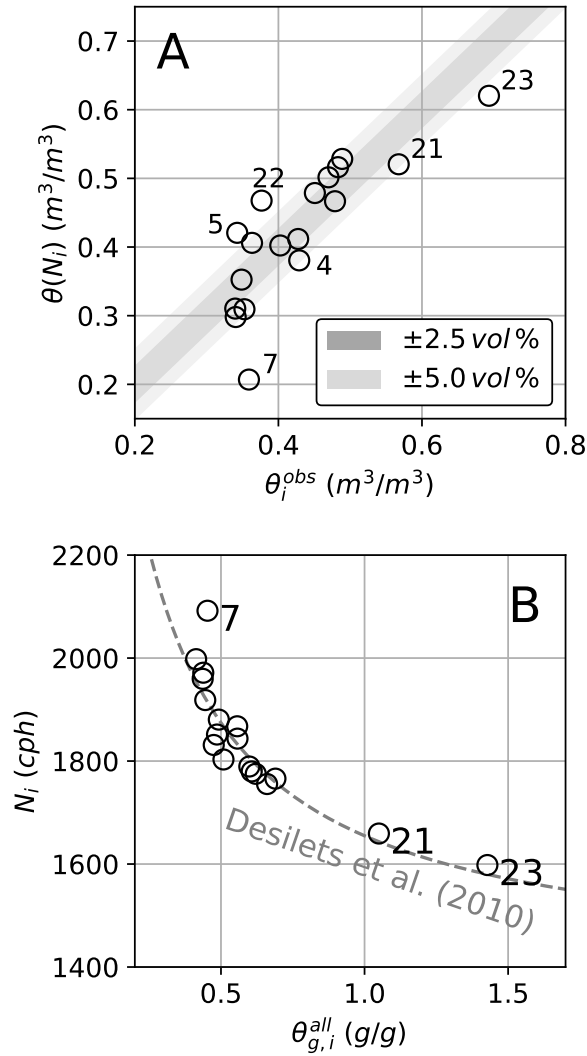
Figure 3. Results of the N_0 calibration: the upper panel shows the $\theta(N_i)$ as obtained from standardized and corrected neutron count rates N_i versus conventional soil moisture estimates θ_i^{obs}, i.e. footprint-averaged volumetric soil moisture obtained from manual sampling (June 25-26, 2019). The grey shadows indicate a deviation of 2.5 and 5 % in $\theta(N_i)$. The bottom panel provides a different perspective by plotting N_i versus the observed total gravimetric soil water content, including water equivalents from soil organic matter and lattice water; the dashed line indicates the Desilets function, Eq. 1, with a calibrated N_0=3723 cph.

boxes which represent the inter-quartile ranges of $\theta(N_i)$, θ_i^{obs}, and N_i, clearly overlap with the diagonal (Fig. 4A), and mostly with the curve of the Desilets function, respectively (Fig. 4B).

Only for CRNS sensor 7, the box does neither connect to the diagonal nor to the Desilet function, so we cannot assume that the N_0 value of 3723 cph is valid for this CRNS location. Currently, we do not have a satisfactory explanation: the uncertainties

17

Table 2. Overview of calibration data and results per sensor (variables with an asterisk (*) were computed as a weighted average per footprint). ID: sensor ID, Forest: Percentage of forest area in the footprint; AGB: above-ground dry matter biomass; N: corrected neutron count rates, averaged over calibration period; ρ_b: soil bulk density (note that the vertical weighting gives more weight to the top soil where bulk density tends to be lower, cf. section 4.1.4 and Fig. S2 in the supplementary); SOM: soil organic matter content; θ^{obs}: volumetric soil water content from manual measurements; θ^{eq}: volumetric soil water equivalent ($\theta^{som} + \theta^{lw}$; $\theta(N)$: volumetric soil water content as estimated from Eq. 1.

ID	Forest	AGB *	N	ρ_b *	SOM *	θ^{obs} *	θ^{eq} *	$\theta(N)$
	(%)	(kg/m^2)	(cph)	(kg/l)	(kg/kg)	(m^3/m^3)	(m^3/m^3)	(m^3/m^3)
1	73	18.2	1775	0.96	0.15	0.48	0.11	0.52
2	0	0.4	1959	1.06	0.15	0.34	0.12	0.31
3	0	0.1	1971	1.07	0.14	0.35	0.12	0.31
4	2	0.6	1867	1.01	0.17	0.43	0.13	0.38
5	0	0.4	1831	0.93	0.13	0.34	0.10	0.42
6	17	4.0	1880	1.07	0.15	0.40	0.12	0.40
7	0	0.2	2091	1.07	0.15	0.36	0.12	0.21
8	0	0.1	1789	0.92	0.14	0.45	0.10	0.48
14	92	20.8	1851	0.98	0.15	0.36	0.11	0.41
16	9	2.6	1843	0.96	0.14	0.43	0.11	0.41
17	1	0.4	1765	0.82	0.13	0.48	0.09	0.47
18	1	0.6	1755	0.86	0.15	0.47	0.10	0.50
19	85	13.6	1779	0.99	0.15	0.49	0.11	0.53
21	6	2.1	1659	0.69	0.37	0.57	0.16	0.52
22	88	21.5	1803	0.95	0.14	0.38	0.11	0.47
23	19	4.7	1598	0.56	0.31	0.69	0.10	0.62
24	0	0.1	1997	1.13	0.14	0.34	0.13	0.30
25	0	0.1	1918	1.03	0.13	0.35	0.11	0.35

of vegetation biomass, soil organic matter, or lattice water around sensor 7 cannot explain the level of disagreement, and the

405   standardization of sensitivity for sensor 7 appears to be successful (the neutron intensity from sensor 7 corresponds well to the rover measurement, see Fig. S4). It is possible, though, that the reference soil moisture θ_7^{obs} is too high: the soils appear to become drier towards the west, and a preliminary analysis of roving data from June 2019 indicates relatively dry conditions along the road south-west of sensor 7 (see Fig. 10 in Fersch et al., 2020a). At the same time, manual measurements were specifically scarce in the western footprint of sensor 7 (due to access restrictions and technical issues which led to the loss of

410   manual FDR profiles at five locations), so that our estimate θ_7^{obs} might in fact not be representative for the footprint. Still, we do not have hard evidence to support this hypothesis, so we decided to exclude sensor 7 from further analysis in the present study.
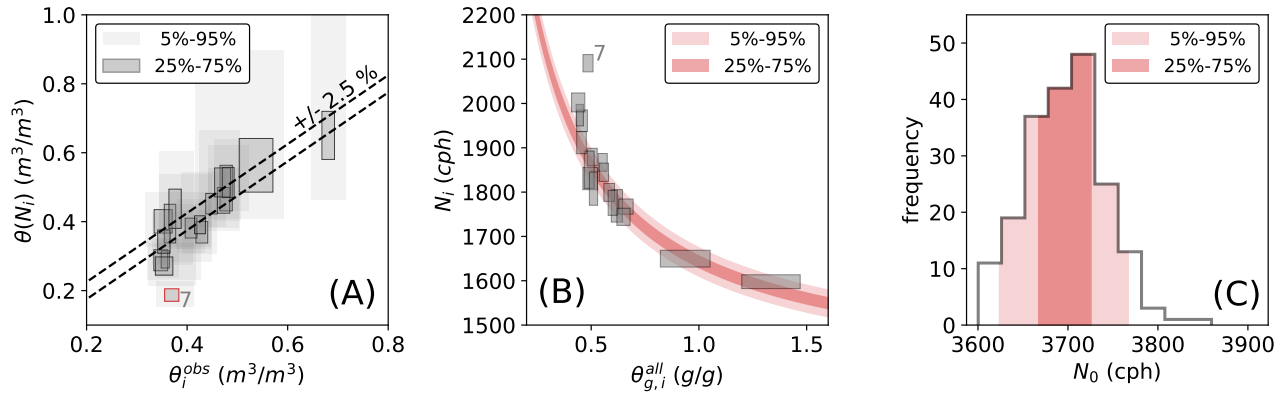
Figure 4. Results of the Monte-Carlo-analysis: (A) shows $\theta(N_i)$ versus θ_i^{obs}, while the (B) shows corrected neutron intensities N_i over the gravimetric soil water equivalent $\theta_{g,i}^{all}$. The dark grey shades represent the inter-quartile range of these variables based on the 200 realisations in the Monte-Carlo analysis. In their horizontal and vertical extent, we use these dark shades to measure the "local uncertainty" of these variables where the term "local" refers to the uncertainty for a specific sensor footprint i; the light grey shades (in (A) only) show the inner 90 % of realization for illustrative purposes only. (C) shows the distribution of all 200 N_0 values, highlighting the inter-quartile range in dark and the inner 90 % in light red, respectively. Accordingly, the red shades in (B) indicate the ranges of the Desilets function when using the inter-quartile range or the inner 90 % of N_0 realisations.

5.2 Spatial and temporal patterns in CRNS-based soil moisture

We used the joint N_0 value together with a 12-hours moving average of the corrected neutron intensities and Eq. 1 to retrieve

415   time series of volumetric soil moisture for the remaining 17 locations and over the entire study period (Fig. 5).

Overall, we see strong temporal dynamics of wetting, drying, and re-wetting that correspond well with the cumulative difference between precipitation and reference evapotranspiration (red line in the top panel of Fig. 5). Torrential rains of about 150 mm from May 20-22 marked the start of the campaign, with another 50 mm of rain until May 29. During that period, volumetric soil moisture exceeded the soil porosity in many locations (marked by the black + signs). That is in line with the

420   observation that large parts of the study area were affected by ponding in the last week of May. The following drying period until July 15 was repeatedly interrupted by rainfall events of more than 10 mm (e.g. on June 15 and 20, July 1, 7 and 12). Still, June marks the transition from saturated to moderately dry conditions: from June 1 to 30, soil moisture dropped by 0.2 - 0.3 m^3/m^3 for each CRNS location (a decrease between 25 to 50 percent relative to the soil moisture on June 1).

The rows in the bottom panel of Fig. 5 have been sorted in descending order, from top to bottom, based on the average soil

425   water content during the last week of the campaign (July 8-15). From that arrangement, some patterns in space and time emerge. Location 23, located in a large patch of peat soil, stands out with a very high soil moisture permanently above 0.5 m^3/m^3 (with an average of 0.71 m^3/m^3). At the other end, there is a group of relatively dry locations in the western parts of the study area (locations 2, 3, 4, 24, and 25), and, less pronounced, but still rather dry, along the eastern slopes towards the water divide of the catchment (locations 6, 14, and 16). In-between, we find a series of locations with intermediate soil moisture levels and
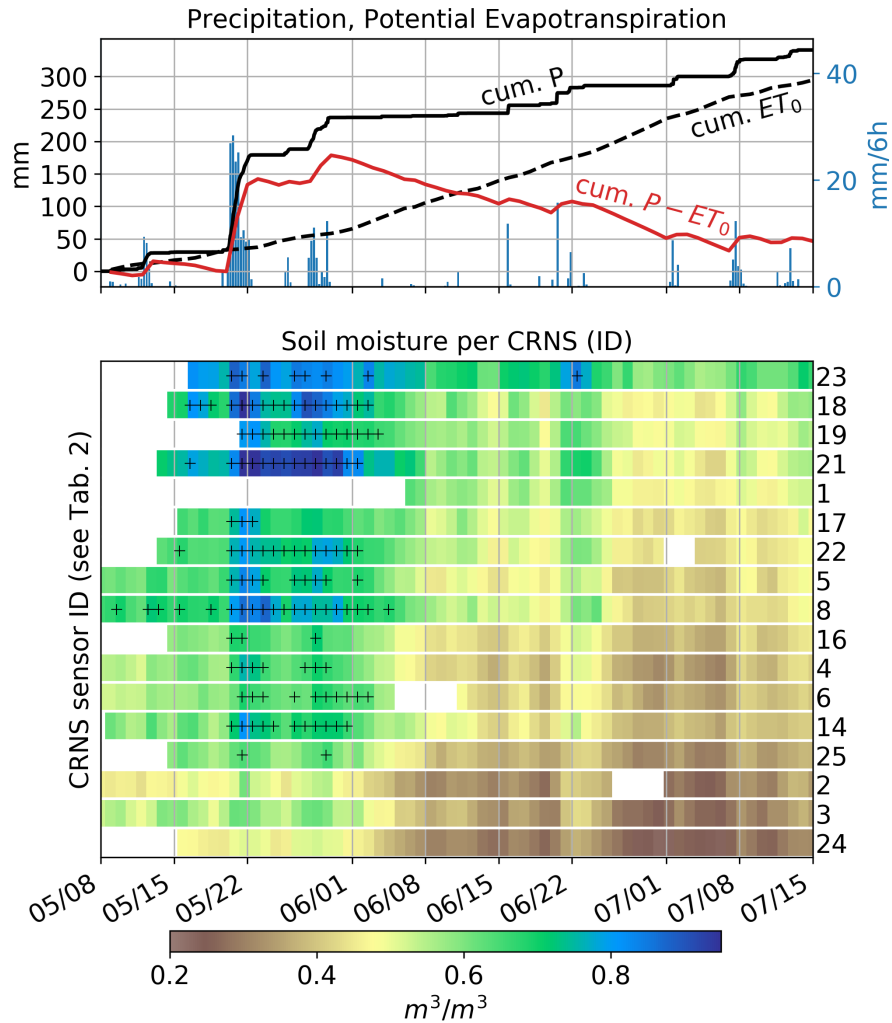
Figure 5. Time-series of precipitation, reference evapotranspiration, and estimated soil water content. Top: cumulative values of precipitation P (mm), reference evapotranspiration ET_0 (based on FAO, 1998, in mm), and the difference $P - ET_0$ (in mm); precipitation depth (mm) per 6 hour intervals (blue bars). Bottom: soil moisture $\theta(N_i)$ as estimated for each CRNS sensor i; rows are sorted in descending order, from top to bottom, based on the average soil water content during the last week of the campaign (July 8-15). A white space indicates a period of missing data, the black "+" signs indicate periods in which the apparent volumetric soil moisture exceeds soil porosity, probably due to ponding.

430   pronounced wetting and drying dynamics over the study period, most of them strung along the central valley bottom of the Rottgraben (locations 1, 5, 17, 18, and 21) as well as a drainage line from the eastern slopes (location 19). Location 8 is more peculiar: it is very close to the driest locations, starts off very wet, but also exhibits pronounced drying dynamics.

We have to keep in mind the results from section 5.1, which indicated the large local uncertainty of $\theta(N)$. Hence, any ranking that is based on average soil moisture values should be interpreted with care. Take location 22, for instance: Fig. 3 suggests that $\theta(N)$ is probably overestimating soil moisture in this location which is supported by the uncertainty range shown in Fig. 4. The dominant source of uncertainty at location 22 is most likely the above-ground forest biomass in the near range of sensor 22. Hence, location 22 could be by around $0.1\,m^3/m^3$ drier than shown in Fig. 5. Examining, however, the way a CRNS location changes rank over time - relative to other locations - should be less affected by such local (but presumably static) uncertainties. From a hydrological perspective, it might be informative to examine such changes in rank as they may indicate changes in governing hydrological processes. As an example, location 21 was by far the wettest location in the last week of May, but only the fourth wettest location in the last week of the campaign. Same as location 23, location 21 is characterised by peaty soils with low bulk density and high soil moisture, but it dries much faster. We hypothesize that during the heavy rainfall in May, location 21 collected near-surface inter-flow from the nearby eastern hillslopes which, in combination with a local impermeable layer below the peat soils, led to a local accumulation of water. However, location 21 might not be influenced as much by the shallow aquifer as location 23, so it dried faster. While this hypothesis remains yet untested, it illustrates how a dense network of CRNS sensors in a heterogeneous landscape could help us to identify governing hydrological processes.

5.3 How does soil moisture vary within and between the sensor footprints?

5.3.1 Spatial interpolation of CRNS-based soil moisture

With this study, we aim at using CRNS data to coherently and continuously represent the catchment-scale variation of soil water content at a resolution of tens to hundreds of meters, i.e. the variation *within* and *between* CRNS footprints. To obtain daily soil moisture maps, we applied two interpolation models (section 4.4), "unconstrained" and "constrained", for each day of the campaign. Fig. 6 shows the exemplary maps for three different dates: a very wet condition on June 1 (two days after the continued rainfall in May 2019 had ended); intermediate wetness on June 7 (after a week of drainage and evapotranspiration); and a relatively dry condition on June 30 (after another three weeks of drying).

For both interpolation models, the maps illustrate more intuitively what we have already learned in the previous section (section 5.2: soils are becoming considerably drier from the valley bottom of the Rottgraben towards the western parts, and, less pronounced, but still obvious, towards the eastern hillslopes. Furthermore, the locations of sensor 19 (at a drainage line) and 8 (in the SoilNet area) are rather wet. The maps also illustrate well how the drying of soils progresses in space in during June. At the same time, Fig. 6 demonstrates the differences between the two interpolation models: as expected, the constrained model enhances horizontal soil moisture gradients (increased contrasts in the bottom panel maps).

The interpolation also allows us to compute a catchment-wide soil moisture average, or to capture the frequency distribution of soil moisture values in the catchment at any point in time. Fig. 7, for instance, shows the median, as well as the inner 50 % and 90 % of the catchment-wide soil moisture values for both interpolation models. While the median values are almost identical, the models clearly differ at the tails of the distribution (most clearly for the 5th and 95th percentile) – a consistent behaviour as the constrained interpolation is expected to enhance gradients.
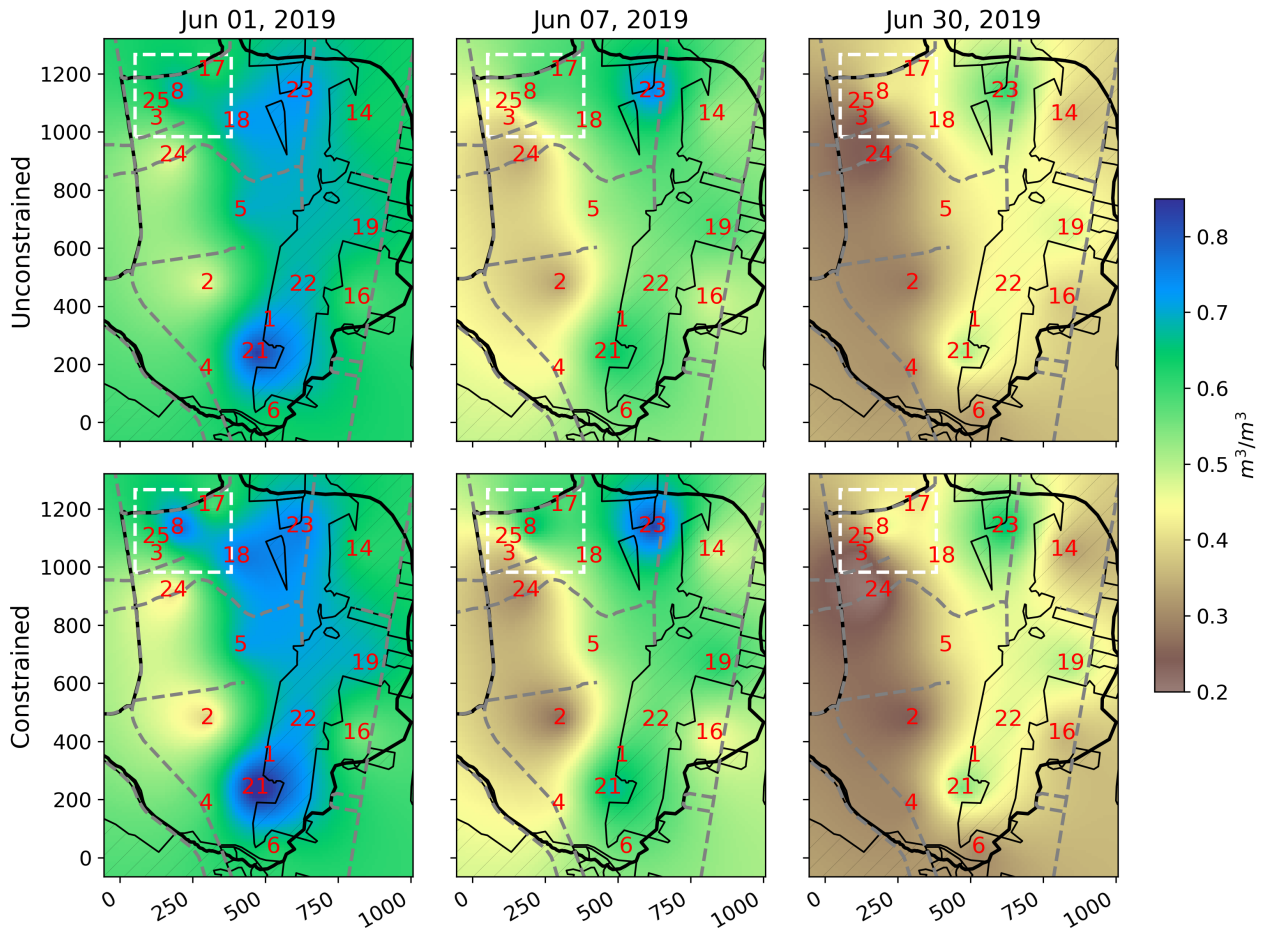
Figure 6. Daily average soil moisture for three different dates (left: June 1, center: June 7, right: June 30, 2019) and for unconstrained/constrained interpolation model (top/bottom row); also shown: locations and IDs of the CRNS sensors used for the interpolation (red), catchment boundary (black line), forest (grey hatches with black contour), roads (dashed grey line), extent of the SoilNet (white dashed rectangle). Figure uses OSM basemap layers for landuse, and roads (© OpenStreetMap contributors, 2020, distributed under ODbL license).

5.3.2 Comparison of spatial patterns against SoilNet observations

The area of the SoilNet is particularly suited to compare the the interpolation models regarding their ability to represent soil moisture gradients: first, the SoilNet allows to capture variability in space due to its high sampling density. Second, the density of CRNS sensors is also higher in that area: the 150 m radii of six sensors (3, 8, 17, 18, 24, 25) substantially overlap with the SoilNet area. Third, the spatial heterogeneity of soil moisture in the SoilNet area appears quite pronounced (generally drier towards the west, together with a wet anomaly at the center).
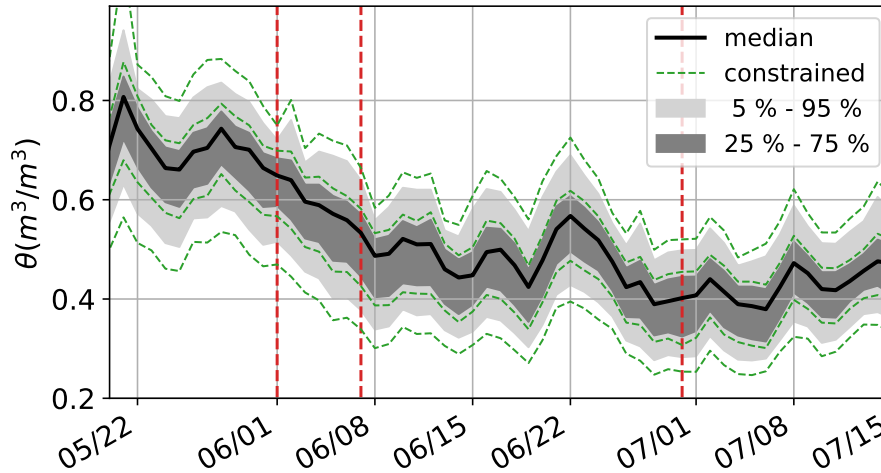
470

Figure 7. Catchment-wide median (black line), inter-quartile range (dark shadow), and inner 90 % (light shadow) of daily soil moisture as obtained from unconstrained interpolation; The dashed green lines indicate the corresponding percentiles (5th, 25th, 75th, and 95th) as obtained from constrained interpolation (the median is not shown in addition as it is almost identical); red dashed lines: dates used in Fig. 6.
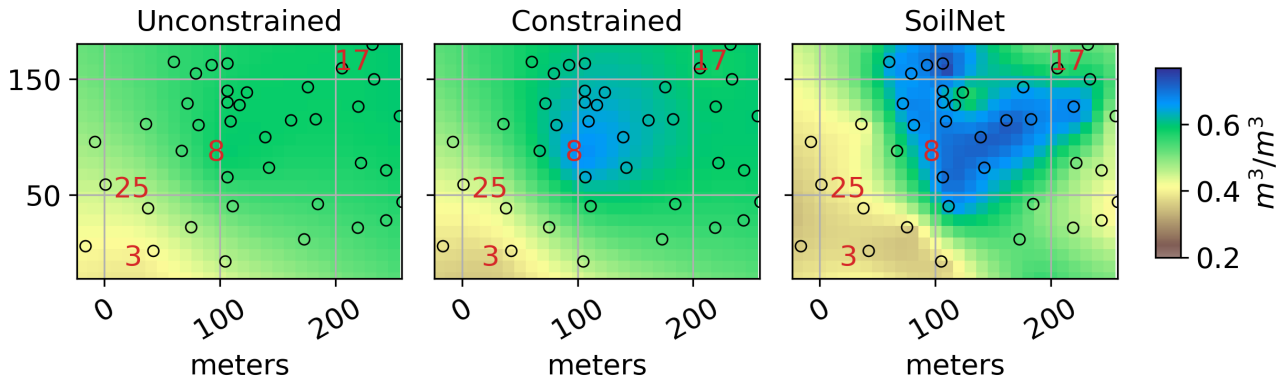

Figure 8. Daily average soil moisture in the SoilNet area on June 7, 2019, as obtained from the unconstrained interpolation (left panel), the constrained interpolation (center panel), and the interpolated SoilNet measurements (right panel). The spatial window corresponds to the dashed white box in Fig. 6. Black circles: locations of the SoilNet nodes; red numbers: CRNS sensor locations and IDs.

For the comparison, we horizontally interpolated the vertically averaged FDR measurements to the same grid as used before (section 4.5), and used only those parts of the grid that fall inside the spatial bounding box of the SoilNet. Fig. 8 shows an example for June 7, 2019 (intermediate wetness conditions): the SoilNet shows a wet area in its central part that tends to extend
475 to the north and the northeast, and a pronounced progression towards drier conditions in the southwest and east. The soil
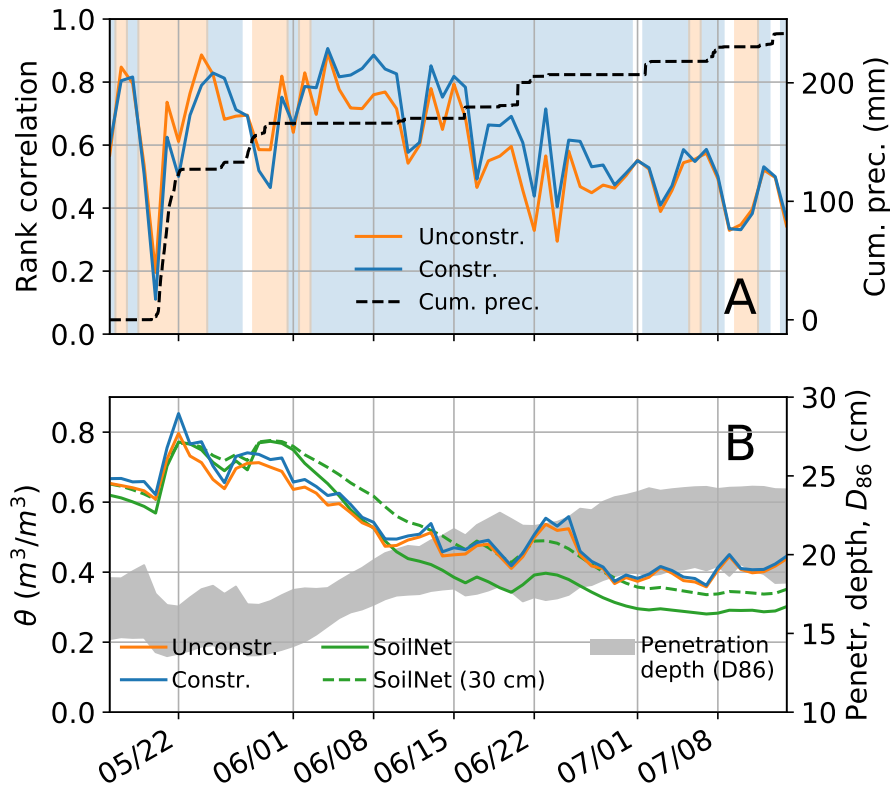
23

Figure 9. (A) The orange (blue) line shows the rank correlation between the daily average soil moisture pattern of the SoilNet and the pattern from the unconstrained (constrained) interpolation of $\theta(N)$; blue/orange backgrounds highlight days on which one model outperforms the other; the dashed black line shows the cumulative precipitation. **(B)** Average daily soil moisture across the SoilNet area as obtained from the unconstrained/constrained interpolation (orange/blue), the vertically-weighted SoilNet observations (solid green), and an unweighted vertical average of the upper 30 cm (dashed green); the grey shade represents the range of penetration depths (D86, the depth within which 86% of neutrons probed the soil) in the footprints from those six CRNS sensors which were closest to the SoilNet area (CRNS 3, 8, 17, 18, 24, 25).

moisture gradient from the center to the south-west is fairly well captured by the constrained interpolation model, particularly in comparison to the unconstrained model; both models fail to reproduce the dry region at the eastern edge.

In order to formalize the comparison, Fig. 9A shows Spearman's rank correlation between the daily spatial soil moisture patterns. Apparently, the constrained model is superior, i.e. more similar to the SoilNet, for the majority of the study period, namely all June. Only for the very wet beginning of the campaign (until early June), the unconstrained model seems to outperform the constrained one. That period, however, has to be interpreted with care since it was governed by substantial ponding, which obviously cannot be captured by the SoilNet sensors, while being detected by the CRNS network. We can also observe a general decline of correlation between the CRNS-based interpolation products and the SoilNet towards the (drier) end of the campaign: in July, the differences in rank correlation between both interpolation models are rather negligible. Rainfall events

485 tend to reduce the correlation which is a well-known issue when using subsurface sensors as a reference: until the infiltration of a rainfall advances to the upper SoilNet sensor (in 5 cm depth), the SoilNet does not register the event while the CRNS sensors immediately react to the additional water at the soil surface, even more while it is close to the surface (Schrön et al., 2017; Scheiffele et al., 2020).

With regard to the *spatial average* of daily soil moisture across the SoilNet area (Fig. 9B), the differences between the
490 two interpolation models are rather negligible, particularly in comparison to the their disagreement with the SoilNet. That fact alone is unsurprising: the constrained model, compared to the unconstrained, enhances spatial gradients, but should not systematically affect the spatial average (section 5.3.1). But what causes the disagreement between the SoilNet average $\langle \theta^{\mathrm{FDR}} \rangle$ and the CRNS-based averages $\langle \theta(N) \rangle$, a disagreement that increases over June? So far, the reasons remain unclear, but we would like to mention three uncertainties: first, the SoilNet measurements at 5, 20 and 50 cm only allow for an imprecise
495 characterisation of the vertical soil moisture profile, specifically in the dynamic upper 20 cm that affect the CRNS signal the most; second, any bias in the conversion from permittivity to volumetric soil moisture might not be homogeneous across the observed range of soil moisture or soil properties in the SoilNet area (section 4.5); and, third, the weighting functions which were used to compute the vertical average θ_n^{FDR} are not necessarily transferable to situations of pronounced horizontal and vertical heterogeneity (Köhli et al., 2015), and hence a known source of substantial uncertainty (Baroni et al., 2018).
500 For illustrative purposes, Fig. 9B shows the range of computed penetration depths (D86) for six nearby CRNS sensors: D86 varies from 14-19 cm in May to about 19-24 cm in July. However, if we average θ^{FDR} uniformly over the upper 30 cm (dashed green line), the agreement with the CRNS-based averages appears somewhat better. The reasons for this behaviour remain unclear, but it emphasizes the possible uncertainty regarding the vertical representativeness of both the CRNS and the SoilNet observations.
505 So while we provided evidence that the constrained interpolation model captures horizontal soil moisture gradients better than the unconstrained model, the usefulness of the SoilNet observations in Fendt as reference data appears to be limited by a range of uncertainties. Future studies might address this issue by exploring other reference data for such benchmark experiences, e.g. roving transects as published by Fersch et al. (2020a).

6 Summary and conclusions

510 This study is the first attempt to analyse the observations of a dense CRNS network in a catchment of $1 \, \mathrm{km}^2$. Based on a comprehensive homogenization, we demonstrated the possibility to retrieve soil moisture using a joint N_0 value, to capture characteristic spatio-temporal features of soil moisture in the study area, and to combine elements from spatial interpolation and geophysical inversion in order to coherently, consistently and continuously represent catchment-scale soil moisture patterns. In the following, we will highlight main lessons as well as theoretical and practical implications for future research.

515 – **The standardization of sensitivity is a vital - but expensive.** Collocating a calibrator probe with most CRNS sensors allowed to make neutron counts comparable across different sensor models (which was independently verified by using a roving CRNS, section S2). That approach is, however, resource-intensive: a person has to move the calibrator, but only

after a minimum of 24 hours. It would therefore be helpful, in the future, to systematically collect and publish sensitivity measurements and sensor inter-comparisons to represent the variability of sensitivity between sensor types, but also within the same sensor type. Assuming reasonable temporal stability, such a database could support standardization of sensitivity in heterogeneous networks, and help to quantify corresponding uncertainties.

– **A joint N_0 is a necessary step towards generalization.** Our study area features considerable heterogeneity in a single square kilometer: organic vs. mineral soils, forest patches (with diverse species and age structures) vs. grassland, a flat valley bottom vs. uphill areas, and complex subsurface structures causing episodically perched groundwater. This heterogeneity made it challenging to eliminate the effects of hydrogen pools other than soil moisture, and to capture the reference soil moisture required for N_0 calibration. Compared to previous experiments with single CRNS sensors, the manual soil sampling campaign was rather sparse due to limited resources. However, the estimation of a joint N_0 helped to address these challenges: it prevented us from overemphasizing specific (uncertain) features in the data of individual sensors (in contrast to calibrating each sensor individually); by repeating the N_0 estimation in a Monte-Carlo-analysis, we confirmed the robustness of the N_0 estimate, but also got an idea of the local uncertainties for both the CRNS-based soil moisture estimate, $\theta(N)$, *and* the reference observations, θ^{obs}, that we considered as "ground truth".

– **Dense networks are informative in both space and time.** The added value of a dense CRNS network became particularly apparent as the strong spatial heterogeneity of soil moisture occurred together with pronounced temporal dynamics of wetting and drying. The network captured marked spatial patterns, but also indicated that these patterns were partly time-variant: when we ranked the locations according to their average soil moisture, the ranking of some locations remained rather stable while others showed pronounced changes in rank. Not only might such changes be informative with regard to governing hydrological processes. They also demonstrate the added value of dense networks in comparison to roving CRNS, and the need to carefully scrutinize assumptions on the time-invariance of relative spatial patterns.

– **Dense networks could work towards downscaling and upscaling.** In combination with spatial interpolation techniques, the dense CRNS network was employed to represent soil moisture gradients at the scale of tens to hundreds of meters (within and between CRNS footprints), and to infer the average soil moisture of a $1\,km^2$ catchment. Future network designs could be tailored more towards downscaling (maximize overlap) or towards upscaling (maximize coverage). The latter option could be specifically useful to validate hydrological models or remote sensing products, or to use these for upscaling at a larger scale.

– **The "constrained" model: a starting point for a more general inversion framework in CRNS.** The "constrained" model interpolates $\theta(N)$ under the constraint to maximise the consistency between the observed neutron count rates and the resulting soil moisture field. This way, further spatial detail can be obtained from volume-integrated observations by using our physical understanding of both the observed system and the observation technology itself. Other than a typical "geophysical inversion", the constrained interpolation uses a geostatistical instead of physical model, and a heuristic forward operator instead of a neutron transport model. Still, we provided a proof-of-concept how this approach can add

to the representation of horizontal gradients. The constrained model could hence lead the way towards a more general inversion framework for dense CRNS networks: such a framework could be open to any type of model $m(\mathbf{p})$ to represent our notion of soil moisture variation in space, e.g. parametric relationships between soil moisture and proxy variables, or a distributed hydrological model, depending on the study area and available data. Certainly, the concept should be scrutinized further, e.g. by using additional reference data (e.g. from CRNS roving) for benchmarking, and by refining the forward operator, specifically for conditions of marked vertical and horizontal heterogeneity.

– **Dense CRNS networks are expensive, but feasible in research environments.** They will probably not become a routine monitoring option in the foreseeable future. In research, though, they could constitute an important component at areas of around a square kilometre with say 10-20 CRNS sensors (depending on the research focus and environment). At that scale, the costs for conventional sensor networks tend to become increasingly prohibitive, not to mention the invasive nature of such measurements which also makes them less versatile in access-limited settings (e.g. agricultural fields). Dense CRNS networks can become particularly feasible if implemented in concerted campaigns, which allows research institutions to combine their resources for instrumentation as well as ground truthing.

Certainly, this study required some fairly arbitrary decisions, e.g. the choice of interpolation techniques, assumptions on the spatial representativeness of measured variables, the sources and ranges of uncertainty, and more. Step by step, this arbitrariness needs to be brought down in future research. But despite these degrees of freedom, we demonstrated how dense CRNS networks can become another valuable option in soil moisture monitoring and hydrological research.

Code and data availability.

The data used in this study are accessible at EUDAT (Fersch et al., 2020b), and described in Fersch et al. (2020a). The data analysis is documented in a Jupyter notebook (https://github.com/cosmic-sense/jfc1-analysis-hess,, Heistermann, 2021).

Author contributions.

MH and TF designed the study, MH wrote the manuscript, TF, MS and SO co-designed the study and co-wrote the manuscript. SO had proposed the concept of a dense CRNS network.

Competing interests. The authors declare that they have no competing interests.

References

Andreasen, M., Jensen, K. H., Desilets, D., Franz, T. E., Zreda, M., Bogena, H. R., and Looms, M. C.: Status and Perspectives on the Cosmic-Ray Neutron Method for Soil Moisture Estimation and Other Environmental Science Applications, Vadose Zone Journal, 16, https://doi.org/10.2136/vzj2017.04.0086, 2017.

Baatz, R., Bogena, H. R., Hendricks-Franssen, H.-J., Huisman, J. A., Montzka, C., and Vereecken, H.: An empirical vegetation correction for soil water content quantification using cosmic ray probes, Water Resources Research, 51, 2030–2046, https://doi.org/10.1002/2014WR016443, 2015.

Baroni, G. and Oswald, S. E.: A scaling approach for the assessment of biomass changes and rainfall interception using cosmic-ray neutron sensing, Journal of Hydrology, 525, 264–276, https://doi.org/10.1016/j.jhydrol.2015.03.053, 2015.

Baroni, G., Scheiffele, L. M., Schrön, M., Ingwersen, J., and Oswald, S. E.: Uncertainty, sensitivity and improvements in soil moisture estimation with cosmic-ray neutron sensing, Journal of Hydrology, 564, 873–887, https://doi.org/10.1016/j.jhydrol.2018.07.053, 2018.

Bayerisches Landesamt für Umwelt: Übersichtsbodenkarte TK25-Blatt 8132, www.lfu.bayern.de, 2014.

Blöschl, G. and Grayson, R.: Spatial Observations and Interpolation, in: Spatial Patterns in Catchment Hydrology - Observations and Modelling, edited by Blöschl, G. and Grayson, R., chap. 2, pp. 17–50, Cambridge University Press, Cambridge, 2000.

Bogena, H. R., Huisman, J. A., Baatz, R., Hendricks-Franssen, H.-J., and Vereecken, H.: Accuracy of the cosmic-ray soil water content probe in humid forest ecosystems: The worst case scenario, Water Resources Research, 49, 5778–5791, https://doi.org/10.1002/wrcr.20463, 2013.

Desilets, D., Zreda, M., and Ferré, T. P. A.: Nature's neutron probe: Land surface hydrology at an elusive scale with cosmic rays, Water Resources Research, 46, https://doi.org/10.1029/2009WR008726, 2010.

Evans, J. G., Ward, H. C., Blake, J. R., Hewitt, E. J., Morrison, R., Fry, M., Ball, L. A., Doughty, L. C., Libre, J. W., Hitt, O. E., Rylett, D., Ellis, R. J., Warwick, A. C., Brooks, M., Parkes, M. A., Wright, G. M. H., Singer, A. C., Boorman, D. B., and Jenkins, A.: Soil water content in southern England derived from a cosmic-ray soil moisture observing system - COSMOS-UK, Hydrological Processes, 30, 4987–4999, https://doi.org/10.1002/hyp.10929, 2016.

FAO: Crop evapotranspiration - Guidelines for computing crop water requirements - FAO Irrigation and drainage paper 56, Tech. rep., FAO, 1998.

Fersch, B., Jagdhuber, T., Schrön, M., Völksch, I., and Jäger, M.: Synergies for Soil Moisture Retrieval Across Scales From Airborne Polarimetric SAR, Cosmic Ray Neutron Roving, and an In Situ Sensor Network, Water Resources Research, 54, 9364–9383, https://doi.org/10.1029/2018wr023337, 2018.

Fersch, B., Francke, T., Heistermann, M., Schrön, M., Döpper, V., Jakobi, J., Baroni, G., Blume, T., Bogena, H., Budach, C., Gränzig, T., Förster, M., Güntner, A., Hendricks-Franssen, H.-J., Kasner, M., Köhli, M., Kleinschmit, B., Kunstmann, H., Patil, A., Rasche, D., Scheiffele, L., Schmidt, U., Szulc-Seyfried, S., Weimar, J., Zacharias, S., Zreda, M., Heber, B., Kiese, R., Mares, V., Mollenhauer, H., Völksch, I., and Oswald, S.: A dense network of cosmic-ray neutron sensors for soil moisture observation in a pre-alpine headwater catchment in Germany, Earth System Science Data, 12, 2289–2309, https://doi.org/10.5194/essd-12-2289-2020, 2020a.

Fersch, B., Francke, T., Heistermann, M., Schrön, M., and Döpper, V.: A massive coverage experiment of cosmic ray neutron sensors for soil moisture observation in a pre-alpine catchment in SE-Germany (part I: core data) [post-review version], https://doi.org/10.23728/b2share.282675586fb94f44ab2fd09da0856883, 2020b.

Gao, F. and Han, L.: Implementing the Nelder-Mead simplex algorithm with adaptive parameters, Computational Optimization and Applications, 51, 259–277, 2012.

615 Heistermann, M.: v2.0 cosmic-sense/jfc1-analysis-hess: After major revision of the manuscript, https://doi.org/10.5281/zenodo.4438921, https://doi.org/10.5281/zenodo.4438921, 2021.

Kiese, R., Fersch, B., Bassler, C., Brosy, C., Butterbach-Bahlc, K., Chwala, C., Dannenmann, M., Fu, J., Gasche, R., Grote, R., Jahn, C., Klatt, J., Kunstmann, H., Mauder, M., Roediger, T., Smiatek, G., Soltani, M., Steinbrecher, R., Voelksch, I., Werhahn, J., Wolf, B., Zeeman, M., and Schmid, H.: The TERENO Pre-Alpine Observatory: Integrating Meteorological, Hydrological, and Biogeochemical Measurements

620 and Modeling, Vadose Zone Journal, 17, https://doi.org/10.2136/vzj2018.03.0060, 2018.

Köhli, M., Weimar, J., Schrön, M., and Schmidt, U.: Moisture and humidity dependence of the above-ground cosmic-ray neutron intensity, Frontiers in Water, 2, 66, https://doi.org/10.3389/frwa.2020.544847, 2020.

Köhli, M., Schrön, M., Zreda, M., Schmidt, U., Dietrich, P., and Zacharias, S.: Footprint characteristics revised for field-scale soil moisture monitoring with cosmic-ray neutrons, Water Resources Research, 51, 5772–5790, https://doi.org/10.1002/2015WR017169, 2015.

625 Landesamt für Digitalisierung, Breitband und Vermessung: Bodenschätzung, https://geoservices.bayern.de/wms/v1/ogc_alkis_bosch.cgi?, 2018.

Mohamed, A.-M. O. and Paleologos, E. K.: Chapter 16 - Dielectric Permittivity and Moisture Content, in: Fundamentals of Geoenvironmental Engineering, edited by Mohamed, A.-M. O. and Paleologos, E. K., pp. 581–637, Butterworth-Heinemann, https://doi.org/https://doi.org/10.1016/B978-0-12-804830-6.00016-8, https://www.sciencedirect.com/science/article/pii/

630 B9780128048306000168, 2018.

OpenStreetMap contributors: Planet dump retrieved from https://planet.osm.org , https://www.openstreetmap.org, 2020.

Schattan, P., Baroni, G., Oswald, S. E., Schoeber, J., Fey, C., Kormann, C., Huttenlau, M., and Achleitner, S.: Continuous monitoring of snowpack dynamics in alpine terrain by aboveground neutron sensing, Water Resources Research, 53, 3615–3634, https://doi.org/10.1002/2016WR020234, 2017.

635 Scheiffele, L. M., Baroni, G., Franz, T. E., Jakobi, J., and Oswald, S. E.: A profile shape correction to reduce the vertical sensitivity of cosmic-ray neutron sensing of soil moisture, Vadose Zone Journal, 19, e20 083, https://doi.org/10.1002/vzj2.20083, 2020.

Schrön, M., Zacharias, S., Köhli, M., Weimar, J., and Dietrich, P.: Monitoring Environmental Water with Ground Albedo Neutrons from Cosmic Rays, in: The 34th International Cosmic Ray Conference, vol. 236, p. 231, SISSA Medialab, https://doi.org/10.22323/1.236.0231, 2016.

640 Schrön, M., Zacharias, S., Womack, G., Köhli, M., Desilets, D., Oswald, S. E., Bumberger, J., Mollenhauer, H., Kögler, S., Remmler, P., Kasner, M., Denk, A., and Dietrich, P.: Intercomparison of cosmic-ray neutron sensors and water balance monitoring in an urban environment, Geoscientific Instrumentation, Methods and Data Systems, 7, 83–99, https://doi.org/10.5194/gi-7-83-2018, 2018.

Schrön, M., Köhli, M., Scheiffele, L., Iwema, J., Bogena, H. R., Lv, L., Martini, E., Baroni, G., Rosolem, R., Weimar, J., Mai, J., Cuntz, M., Rebmann, C., Oswald, S. E., Dietrich, P., Schmidt, U., and Zacharias, S.: Improving calibration and validation of cosmic-ray neutron

645 sensors in the light of spatial sensitivity, Hydrology and Earth System Sciences, 21, 5009–5030, https://doi.org/10.5194/hess-21-5009-2017, 2017.

Schrön, M., Rosolem, R., Köhli, M., Piussi, L., Schröter, I., Iwema, J., Kögler, S., Oswald, S. E., Wollschläger, U., Samaniego, L., Dietrich, P., and Zacharias, S.: Cosmic-ray Neutron Rover Surveys of Field Soil Moisture and the Influence of Roads, Water Resources Research, 54, 6441–6459, https://doi.org/10.1029/2017WR021719, 2018.

650 Shuttleworth, J., Rosolem, R., Zreda, M., and Franz, T.: The COsmic-ray Soil Moisture Interaction Code (COSMIC) for use in data assimilation, Hydrol. Earth Syst. Sci., 17, 3205–3217, https://doi.org/10.5194/hess-17-3205-2013, 2013.

SoilNet: SoilNet website, www.soilnet.de, http://www.soilnet.de, accessed: 26.02.2020, 2018.

Stockmann, I.: Biomasseschätzung in einem temperierten Mischwald auf der Basis von Höheninformationen und multitemporalen RapidEye Daten, 2020.

655 Weimar, J., Köhli, M., Budach, C., and Schmidt, U.: Large-Scale Boron-Lined Neutron Detection Systems as a 3He Alternative for Cosmic Ray Neutron Sensing, Frontiers in Water, 2, 16, https://doi.org/10.3389/frwa.2020.00016, 2020.

Zhdanov, M. S.: Chapter 1 - Forward and Inverse Problems in Science and Engineering, in: Inverse Theory and Applications in Geophysics (Second Edition), edited by Zhdanov, M. S., pp. 3–31, Elsevier, Oxford, second edition edn., https://doi.org/https://doi.org/10.1016/B978-0-444-62674-5.00001-3, https://www.sciencedirect.com/science/article/pii/B9780444626745000013, 2015.

660 Zreda, M., Desilets, D., Ferré, T. P. A., and Scott, R. L.: Measuring soil moisture content non-invasively at intermediate spatial scale using cosmic-ray neutrons, Geophysical Research Letters, 35, https://doi.org/10.1029/2008GL035655, 2008.

Zreda, M., Shuttleworth, W. J., Zeng, X., Zweck, C., Desilets, D., Franz, T. E., and Rosolem, R.: COSMOS: the COsmic-ray Soil Moisture Observing System, Hydrology and Earth System Sciences, 16, 4079–4099, https://doi.org/10.5194/hess-16-4079-2012, 2012.